Phase transition of WTAP regulates m^{6}A modification of interferon-stimulated genes

Sihui Cai[1,#], Jie Zhou[2,3,#], Xiaotong Luo[4], Chenqiu Zhang[1], Shouheng Jin[1], Jian Ren[4], Jun Cui[1]

[1] MOE Key Laboratory of Gene Function and Regulation, State Key Laboratory of Biocontrol, School of Life Sciences, Sun Yat-sen University, Guangzhou, Guangdong, 510006, China.

[2] State Key Laboratory of Membrane Biology & Frontier Research Center for Biological Structure, School of Life Sciences, Tsinghua University, Beijing, 100101, Chian.

[3] Tsinghua University-Peking University Joint Center for Life Sciences, Beijing, 100101, China.

[4] State Key Laboratory of Oncology in South China, Cancer Center, Collaborative Innovation Center for Cancer Medicine, School of Life Sciences, Sun Yat-sen University, Guangzhou 510006, China.

[#] These authors contributed equally: Sihui Cai, Jie Zhou.

Correspondence: Jun.Cui (cuij5@mail.sysu.edu.cn)

Abstract

N^6-methyladenosine (m^{6}A) is the most prevalent modification of mRNA which controls diverse physiological processes. Although m^{6}A modification is reported to regulate type I interferon (IFN) responses by targeting the mRNA of IFN-β and the interferon stimulated genes (ISGs), the detailed mechanism of how m^{6}A methyltransferase complex (MTC) responses quickly to conduct the modification on nascent mRNA co-transcriptionally during IFN-β stimulation remains largely unclear. Here, we demonstrate that WTAP, the adaptor protein of m^{6}A MTC, goes through dephosphorylation regulated phase transition from aggregates to liquid droplets under IFN-β stimulation. Phase transition of WTAP mediates the m^{6}A modification of a subset of ISGs mRNA to restrict their expression. In mechanism, we found that formation of aggregates prevents WTAP from binding on the promoter region of ISGs or conducting m^{6}A modification on mRNA in untreated cells. while IFN-β induced WTAP droplets interacts with nucleus-translocated transcriptional factor STAT1 and recruits MTC on the promoter region of ISGs, directing the co-transcriptional m^{6}A modification on ISGs mRNA. Collectively, our findings reveal a novel regulatory role of WTAP phase transition under viral infection to orchestrate dynamic m^{6}A modification with the cooperation of transcriptional factors and MTC, and precisely manipulate signaling pathway.

Keywords: m^{6}A modification, type I interferon, phase separation, WTAP, interferon-stimulated genes

Introduction

Innate immunity is the first defense line against invading pathogens, mainly through the induction of type I interferon (IFN) and IFN-stimulated genes (ISGs)(Goubau, Deddouche, & Reis e Sousa, 2013). Once the production of type I IFN is initiated, the signal should be tightly restricted to maintain the homeostasis of immune responses (Henault et al., 2016; Schneider, Chevillotte, & Rice, 2014). In the past few years, a large number of studies have reported the post-translational modification of signaling molecules that regulate type I IFN signaling, such as phosphorylation (Uddin et al., 2002; Wen Z, Zhong Z, & Jr., 1995), ubiquitination (Cui et al., 2014; Qin et al., 2016) and methylation (Mowen et al., 2001). However, whether post-transcriptional modification of mRNA affects type I IFN responses remains largely unclear.

Methylation at the N^6 position of adenosine (m^6A) is the most pervasive post-transcriptional modification of mRNA. Deposition of m^6A is catalyzed by methyltransferase complex (MTC), including a key adaptor protein Wilm's tumor–associated protein (WTAP) and key catalyze proteins methyltransferase-like 3 (METTL3) and methyltransferase-like 14 (METTL14)(Schapira, 2016). The m^6A-modified RNAs are recognized by YT521B homology (YTH) domain family proteins, including YTHDC1, YTHDC2, YTHDF1, YTHDF2 and YTHDF3. m6A modification are found to raise different cellular processes (Knuckles & Bühler, 2018; Meyer & Jaffrey, 2017), such as differentiation of stem cells (Geula et al., 2015), circadian clock (Zhong et al., 2018), splicing (Z. Zhang et al., 2010), translation (X. Wang et al., 2015) and destabilization of mRNA (X. Wang et al., 2014). Meanwhile, m^6A modification can be reversed by demethylase fat mass and obesity-associated gene (FTO) and AlkB homolog 5 (ALKBH5)(Jia et al., 2011; Zheng et al., 2013). The co-transcriptional m^6A modification is critical for new born mRNA produced by specific stimulation to participate in further physiological activities. m^6A modification of *IFN-β* mRNA was found to repress antiviral responses under infection of various viruses (Rubio, Depledge, Bianco, Thompson, & Mohr, 2018; Winkler et al., 2019), while others reported that m^6A deposition on different subsets of ISGs mRNA resulted in different effects, like promoting the translation of *IFITM1*

mRNA (McFadden et al., 2021) and stabilizing the mRNA of *STAT1* and *IRF1* (L. Wang et al., 2020). Since the precise and timely m^6A modification on mRNA of antiviral genes plays a significant role in finetuning the antiviral responses, the function of non-catalytic protein WTAP and the detailed mechanism of how MTC responses to IFN-β stimulation need to be clarified.

Here, we observed the phase transition from aggregates to liquid droplets of WTAP driven by IFN-β-induced dephosphorylation. Based on the results from WTAP mutation assay, we revealed that under IFN-β stimulation, liquid-phase of WTAP cooperated with transcriptional factor STAT1 to recruit MTC on promoter region of ISGs, mediating the m^6A modification on new born ISGs mRNA and the expression of a subset of ISGs, thus affecting the antiviral type I IFN responses. Our study sheds light on the mechanism that phase transition of WTAP bridges transcriptional factors and MTC to finetune effective m^6A deposition on specific mRNAs.

Results

WTAP undergoes phase separation during IFN-β stimulation

To explore the detailed mechanism of WTAP-directed m^6A modification on ISGs mRNA, we first investigated the expression of WTAP during virus infection. we infected cells by RNA virus VSV or DNA virus HSV-1 and conducted the immunofluorescence experiments. Surprisingly, we found WTAP clustered and formed condensate-like pattern in cells during virus infection (Figure 1A and Figure 1-figure supplement 1A). We then stimulated cells with IFN-β, and found the increasing number of WTAP condensates formation under IFN-β treatment (Figure 1B). Previous studies reported that some components in the methyltransferase complex such as METTL3 or YTHDFs performed liquid-liquid phase separation (LLPS) during m^6A modification process (Han et al., 2022; J. Li et al., 2022), we suspected whether the IFN-β-mediated WTAP condensates indicating the phase separation of WTAP.

We predicted the prion-like domain (PLD) within WTAP using PLAAC websites (http://plaac.wi.mit.edu/) and found a fragment (234-249 amino acids) was predicted as PLD of WTAP, giving a clue that WTAP may have the ability to go through phase separation (Figure 1C and Figure 1-figure supplement 1B). To directly prove the phase separation properties of WTAP *in vitro*, we purified the recombinant mCherry-WTAP protein, mixed recombinant mCherry-WTAP with physiological buffer and found that the buffer became turbid (Figure 1D). Observation under microscope showed that mCherry-WTAP automatically formed liquid-like condensates which could be reversed by 1,6-hexanediol (hex), an inhibitor of phase separation (Figure 1E). Phase diagram of WTAP phase separation is also established under different concentration of potassium chloride and recombinant mCherry-WTAP (Figure 1-figure supplement 1C). Fusion of condensates were observed and larger condensates were formed *in vitro* (Figure 1-figure supplement 1D). These data together confirmed that WTAP underwent phase separation *in vitro*.

To further explore the protein properties, we detected the phase separation behavior of WTAP in cells. Gene expressing mCherry-WTAP was introduced in WTAP-KO HeLa cells to generate mCherry-WTAP-rescued HeLa cells and treat with or without IFN-β stimulation. Results showed a few WTAP condensates occurred in untreated cells and increasing number of WTAP condensates under IFN-β stimulation. After hex treatment, WTAP condensates in both untreated cells or IFN-β treated cells were disrupted to a dispersed pattern (Figure 1F). Similarly, hex treatment in virus-infected cells also disrupted the formation of WTAP condensates (Figure 1A and Figure 1-figure supplement 1A). We next checked the mobility of WTAP condensates by fluorescence recovery after photobleaching (FRAP) experiments. Intriguingly, WTAP showed less recovery intensity in untreated cells, but showed higher mobility with quick recovery intensity in IFN-β treated cells (Figure 1G). These results implied that WTAP also underwent phase separation in cells, and IFN-β mediated the phase transition of WTAP to form the liquid-like droplets physiologically.

In order to figure out the driving force that mediates the phase separation of WTAP, we first detected the function of predicted PLD domain in WTAP. However, deletion

of PLD failed to abolish the phase separation properties of WTAP (Figure 1-figure supplement 2A), showing that PLD-PLD interaction is not necessary for WTAP phase separation. Since previous studies have uncovered that protein phase separation could be controlled by interaction between specific region through multiple factors (Murthy et al., 2019; J. Wang et al., 2018), including electrostatic interaction (Boyko, Qi, Chen, Surewicz, & Surewicz, 2019), hydrophobic contacts (Reichheld, Muiznieks, Keeley, & Sharpe, 2017) or hydrogen bonds (Gabryelczyk et al., 2019), we next tried to figure out such phase separation-driven region of WTAP. We analyzed the net charge per region and hydropathy of WTAP, but no specific domains with opposite charge or high level of hydrophobicity was found (Figure 1-figure supplement 2B-C), indicating that electrostatic interaction and hydrophobic contacts might not be the key driving force for WTAP phase separation. We then analyzed the abundance of amino acids and found that Serine (Ser), Glutamine (Gln), Glutamate (Glu) and Leucine (Leu) were significantly higher than other amino acids within WTAP (Figure 1-figure supplement 2D). Gln and Leu were mainly located in the N-terminal domain (NTD) while Ser was mostly enriched in the C-terminal domain (CTD), implying the different properties of NTD and CTD (Figure 1C). Previous researches reported that hydrogen bond between serine side chain mediated the intermolecular interaction and LLPS of FUS. In addition, abnormal glutamine-repeat resulted in the formation of β-sheet and solid/gel-like aggregates with lower mobility (Perutz, 1996; Tanaka, Morishima, Akagi, Hashikawa, & Nukina, 2001), which were related to neurodegenerative diseases like Huntington's disease (Gourfinkel-An et al., 1997). Therefore, we wondered whether glutamine-rich NTD and serine-rich CTD of WTAP induced the distinct phase separation. As predicted, we found full-length WTAP and CTD WTAP formed liquid droplets, while NTD of WTAP clustered and formed aggregates with lower mobility, which was confirmed through FRAP experiments (Figure 1H and Figure 1-figure supplement 2E). Intriguingly, we further observed that full-length WTAP transited from droplets to aggregates after incubation for several minutes (Figure 1-figure supplement 2F), validating the different phase separation potential of NTD and CTD of WTAP.

IFN-β-mediated dephosphorylation induces the phase transition of WTAP

Since the serine-rich CTD played the key role in liquid droplets formation of WTAP, we wondered whether IFN-β-mediated WTAP phase transition through serine-phosphorylation by electrostatic repulsion among negatively charged phosphate. We detected the phosphorylation level of WTAP through IP assay and found that phosphorylation of WTAP was significantly decreased under IFN-β stimulation (Figure 2A). Through IP assays, we aimed to identify the phosphatases that dephosphorylate WTAP, thus checked the interaction between WTAP and family of protein phosphatases (PPPs), and found that PPP4 presented the strongest interaction with WTAP (Figure 2-figure supplement 1A). IFN-β stimulation promoted the interaction between WTAP and PPP4 (Figure 2B and Figure 2-figure supplement 1B). Consistently, knockdown of PPP4 enhanced the phosphorylation level of WTAP in IFN-β treated cells (Figure 2C), indicating that IFN-β regulated dephosphorylation of WTAP through PPP4.

To validate the effects of phosphorylation on the phase transition of WTAP, we first confirming the phosphorylation site of WTAP by mass spectrometry (MS) assays. MS results identified six phosphorylated serine/threonine sites within WTAP, while five of six phosphorylation sites were located in CTD of WTAP (Figure 2D and Figure 2-figure supplement 1C). We then constructed a series of phosphorylation mimic, serine/threonine to aspartate mutants (S/T-D) or phosphorylation-deficient, serine/threonine to alanine mutant (S/T-A) of WTAP, and observed the phase separation of WTAP mutants *in vitro*. We found that multiple sites (n > 2) with phosphorylation-mimic mutations of WTAP promoted the aggregation, while 5ST-A mutant formed similar liquid droplets as wild type (WT) WTAP (which was unphosphorylated due to the absence of kinase of WTAP `in *E. coli*) (Figure 2E-F and Figure 2-figure supplement 1D). We next conducted FRAP experiments and found that mobility of WTAP wild type (WT) as well as 5ST-A was significantly higher than that of its 5ST-D mutant *in vitro* (Figure 2G). However, hyperphosphorylated WTAP WT in untreated cells showed lower mobility as 5ST-D mutant compared to

phosphorylation-deficient 5ST-A mutant, while IFN-β-induced dephosphorylation promoted the recovery efficiency of WTAP WT as higher as 5ST-A mutants of WTAP (Figure 2H). Additionally, we found liquid droplets of WTAP after IFN-β stimulation was blunted in *PPP4* knocked-down cells (Figure 2-figure supplement 1E-F), revealed that IFN-β triggered PPP4-mediated dephosphorylation of WTAP to control the phase transition of WTAP. Taken together, we concluded that hyperphosphorylation of WTAP tended to form aggregates with low mobility due to electrostatically repulsed between phosphorylated serine sites, while hypophosphorylation of WTAP promotes the mobility and forms liquid droplets. IFN-β-mediated dephosphorylation promotes the transition from aggregates to liquid-phase of WTAP both *in vitro* and in cells (Figure 2I).

Phase transition of WTAP directs m^{6}A modification on ISGs mRNA to regulate ISGs expression

Next, we wanted to figure out how IFN-β-mediated WTAP phase transition functions in ISGs mRNA. Previous reports indicated that m^{6}A modification affected antiviral activity through enhancing stability and translation of ISGs mRNA (McFadden et al., 2021; L. Wang et al., 2020). To verified the function of WTAP on ISGs mRNA m^{6}A modification, we used CRISPR-Cas9 system to construct *WTAP*^{sgRNA} THP-1 cells, and performed the RNA sequencing (RNA-Seq) followed with bioinformatic analysis, and uncovered that 1440 and 1689 genes were up-regulated in response to IFN-β stimulation for 6 and 12 hours respectively (Figure 3A and Figure 3-figure supplement 1A-B), in which expression of 441 ISGs were enhanced in *WTAP*^{sgRNA} cells, and they were mainly enriched in various aspects of immune responses, including *IFIT1*, *IFIT2*, *OAS1* and *OAS2* (Figure 3B-C). We also found that WTAP showed no effect on the phosphorylation level or protein level of STAT1, STAT2 under IFN-β stimulation (Figure 3-figure supplement 1C-D), suggesting that WTAP regulated ISGs expression through other aspect but not the changes on transcriptional factors.

We then collected the mRNA of control and *WTAP*^{sgRNA} cells stimulated with or without IFN-β and performed m^{6}A methylated RNA immunoprecipitation followed by deep sequencing (MeRIP-Seq). Consensus m^{6}A modified core motifs were enriched in our samples and the majority of WTAP-dependent m^{6}A modification peaks were located in CDS and 3'-UTR (Figure 3D-E and Figure 3-figure supplement 1E-F). ISGs that was m^{6}A modified in control cells but diminished in *WTAP*^{sgRNA} cells were clustered in the IFN-associated pathway through MeRIP-seq assays (Figure 3-figure supplement 1G). By MeRIP- quantitative real time-polymerase chain reaction (qPCR) assays, we analyzed and confirmed the m^{6}A modification level of WTAP-downregulated ISGs and found that deficiency of WTAP resulted in decrease of m^{6}A level on ISGs, including *IFIT1*, *IFIT2*, *OAS1* and *OAS2* (Figure 3F). m^{6}A deposition was reported to affect various aspects of RNA, especially for the decay of mRNA (Oerum, Meynier, Catala, & Tisne, 2021; Shi et al., 2017; X. Wang et al., 2014). We then checked the expression and mRNA stabilization of these ISGs by qPCR, and found that lack of m^{6}A modification in *WTAP*^{sgRNA} cells led to the ISGs mRNA stabilization, thus up-regulated the ISGs expression (Figure 3-figure supplement 1H-I).

To further delineate the function of WTAP phase separation on m^{6}A modification, we treated cells with hex to disrupt the phase separation of WTAP, and detected the m^{6}A deposition in cells with virus infection or IFN-β treatment. We found that virus infection or IFN-β stimulation induced m^{6}A modified ISGs mRNA, and their m^{6}A modification was blocked by hex (Figure 3G and Figure 3-figure supplement 2A-B). Additionally, IFN-β-stimulated m^{6}A modification enrichment on ISGs mRNA were inhibited with hex treatment in control cells but not *WTAP*^{sgRNA} cells (Figure 3G). Increased ISGs mRNA stability was also observed with hex treatment in control cells but not *WTAP*^{sgRNA} cells (Figure 3-figure supplement 2C), suggesting the essential role of WTAP phase separation in ISGs mRNA m^{6}A deposition.

Next, we aimed to uncover the distinct ability to direct m^{6}A modification of ISGs between aggregates or liquid-phase separated WTAP. By knocking down PPP4, hyperphosphorylated aggregation of WTAP were maintained under IFN-β stimulation,

and the m^{6}A modification on ISGs mRNA were surprisingly found to be decreased (Figure 3H). Enhanced mRNA level was also detected with PPP4 deficient (Figure 3-figure supplement 2D). We re-introduced WTAP WT, or its 5ST-D or 5ST-A mutant into *WTAP*^{sgRNA} THP-1 cells to generate WTAP WT, WTAP 5ST-D or 5ST-A THP-1 cells respectively (Figure 3-figure supplement 2E). Our results showed that m^{6}A modification level of ISGs in *WTAP*^{sgRNA} and WTAP 5ST-D mutant cells was significantly attenuated than that of control cells, WTAP WT cells and WTAP 5ST-A mutant cells (Figure 3I). Collectively, these results demonstrated that m^{6}A modification of ISGs mRNA was mainly regulated by the liquid-phase separated WTAP that dephosphorylated by PPP4 under IFN-β stimulation.

Liquid-phase separated WTAP recruits MTC and STAT1 on promoter region to direct the m^{6}A modification of ISGs mRNA

Although m^{6}A modification of ISGs have been reported previously, the detailed mechanism of how WTAP directed m^{6}A modification on ISGs mRNA and the distinct mechanism between WTAP aggregates and liquid-phase separated WTAP were still unknown. By checking the expressions of WTAP and other m^{6}A modification-associated molecules, we found they were not significantly affected by IFN-β (Figure 4-figure supplement 1A-B). Previous report showed that m^{6}A modification of TGF-β downstream genes was directed by the interaction between transcriptional factors SMAD2/3 and WTAP (Bertero et al., 2018). Therefore, we wondered whether m^{6}A modification of ISGs mRNA was directed by WTAP and IFN-β-activated transcriptional factors, including STAT1, STAT2 and IRF9,[3] which recruited the m^{6}A methyltransferases for further m^{6}A modification. We predicted the occupancy of the promoters of WTAP-regulated ISGs (2000 bp upstream of genes were analyzed, while 500 bp upstream of genes were considered as the proximal part of promoter) through directing using AnimalTFDB 3.0 website (http://bioinfo.life.hust.edu.cn/AnimalTFDB/) (Hu et al., 2019). Most of the ISGs were occupied by STAT1 rather than STAT2 and IRF9 (Figure 4A), especially for the proximal part of promoter, pointing the possible role of STAT1 in WTAP-induced

m^{6}A modification. We then detected the interaction between WTAP, METTL3 and STAT1 through immunoprecipitation (IP) assay and found that the interaction between WTAP, METTL3 and STAT1 was enhanced under IFN-β stimulation (Figure 4B). Additionally, the interaction between STAT1 and METTL3 was abolished in *WTAP*^{sgRNA} cells (Figure 4C). RIP-qPCR assays showed that interaction between METTL3 and ISGs mRNA was disrupted in *WTAP*^{sgRNA} cells, further validating the involvement and importance of WTAP in METTL3-dependent m^{6}A deposition, and verifying the formation of STAT1-WTAP-METTL3-ISGs mRNA complex under IFN-β stimulation (Figure 4D).

To determine the contribution of phase-separated WTAP, we used hex to inhibit WTAP phase separation and checked its interaction with STAT1. The interaction between WTAP, METTL3 and STAT1 was dramatically inhibited with hex treatment both in cells and *in vitro* (Figure 4E-F, and Figure 4-figure supplement 1C). By immunofluorescence (IF) experiments, we found IFN-β promoted the interaction between WTAP, METTL3 and STAT1 in cells, which could be abolished by hex (Figure 4G and Figure 4-figure supplement 1C). In order to confirm the importance of WTAP in bridging STAT1-METTL3 interaction, we purified the recombinant GFP-STAT1, mCherry-WTAP and CFP-METTL3 using *E. coli* expressing system and detected the condensation among these proteins *in vitro*. We observed that WTAP was able to form condensates with STAT1 or METTL3 alone while condensation of STAT1 and METTL3 was significantly diminished in the absence of WTAP (Figure 4H-I and Figure 4-figure supplement 1D). Consistent with the results in cells, the interaction between WTAP and STAT1 was blunted by hex (Figure 4-figure supplement 1E). Altogether, our data showed that phase separated WTAP functioned as the key adaptor protein bridging METTL3 and STAT1 to direct the m^{6}A modification of ISGs mRNA.

We next tried to figure out how STAT1-MTC bound and mediated m^{6}A modification on ISGs mRNA. By performing the chromosome immunoprecipitation (ChIP)-qPCR experiments, we found that WTAP interacted with promoter region of ISGs along with STAT1 under IFN-β stimulation (Figure 5A-B). Deficient of STAT1

abolished the binding affinity between WTAP and ISGs promoter region (Figure 5C), implying that nucleus-translocated transcriptional factor STAT1 directed WTAP and MTC to promoter region of ISGs to conduct m^6A deposition process on mRNA. By knocking down PPP4 to block the phase transition to liquid droplets of WTAP, we observed the decreased interaction between WTAP and ISGs promoter region in *PPP4* knock-down cells, indicating the binding affinity between WTAP and ISGs promoter region might depend on PPP4-mediated phase transition of WTAP (Figure 5C). In addition, ChIP-qPCR experiments in WT, $WTAP^{sgRNA}$, WTAP WT, 5ST-D and 5ST-A THP-1 cells demonstrated that WTAP 5ST-D mutant showed significant reduced binding ability to ISGs promoter region after IFN-β stimulation compared to that of WTAP WT and WTAP 5ST-A cells (Figure 5D), which were consistent with the m^6A modification results on ISGs mRNA (Figure 3I). These results further validated that phase transition of WTAP was important for the binding ability to ISGs promoter region and the m^6A modification.

Taken together, our findings revealed the driving force of aggregation and liquid droplets formation of WTAP, and demonstrated the distinct function between aggregates and liquid-phase separated WTAP. Based on our findings, we proposed a working model of WTAP phase transition in the regulation of m^6A modification of ISGs mRNA under IFN-β stimulation. WTAP with high phosphorylation state in untreated cells tended to clustered together forming gel-like aggregates with lower mobility, and restricted the interaction between WTAP-dependent MTC and ISGs promoter region. After IFN-β stimulation, protein phosphatase PPP4 mediated the dephosphorylation of WTAP, resulting in the phase transition from aggregates to liquid-phase of WTAP. Liquid-phase of WTAP increased the mobility of WTAP droplets, and recruited METTL3 and nucleus-translocated STAT1 together to form STAT1-WTAP-METTL3 droplets. Leading by transcriptional factor STAT1, the droplets were able to directly bind with ISGs promoter region, and conducted the m^6A modification of ISGs mRNA during the STAT1-mediated transcription process, thereby prompting diverse regulation of ISGs mRNA. Our work uncovered the function of WTAP phase transition physiologically through the cooperation between

gene transcription and mRNA modification, and provided a full picture of multi-layer regulation of ISGs m^6A modification and expression by the phase transition of WTAP (Figure 5E).

Discussion

m^6A deposition is one of the most widespread post-transcriptional modifications, which is involved in various aspects of RNA metabolism to regulate different biological events, including antiviral response (Garcias Morales & Reyes, 2021). WTAP is a key component in MTC. Physiologically, WTAP works as a skeleton protein to recruit and stabilize other MTC components, such as METTL3 and METTL14, into nuclear speckles. Numerous studies have showed that WTAP was essential in embryo development, cell progression and differentiation, antiviral responses and many other physiological activities (Cho et al., 2021; Huang, Mo, Liao, Chen, & Zhang, 2022; X. Jiang et al., 2021). Abnormal expression of WTAP was discovered in multiple diseases, including cancer or diabetes, to address dysfunctional m^6A modification in specific genes (Chen et al., 2019; Huang et al., 2022; Z. X. Li et al., 2022; Yu et al., 2021). However, the understanding of how WTAP builds up MTC, and how it reacts in response to specific stimulation is insufficient.

Phase separation is a well-known phenomenon associated with the formation of membraneless organelles, which concentrates the substrates and enzymes and accelerates biochemistry reactions (Alberti, Gladfelter, & Mittag, 2019). Previous studies reported that METTL3 and YTHDFs underwent LLPS during the m^6A deposition and recognition process (Han et al., 2022; J. Li et al., 2022), while the m^6A modification also promoted the LLPS of RNA-binding proteins, including m^6A-mRNA-YTHDFs and m^6A-eRNA/YTHDC1/BRD4 condensates (Gao et al., 2019; Lee et al., 2021; Ries et al., 2019; J. Wang et al., 2020). But whether other molecules in MTC undergo phase separation and the driving force of their phase separation were still not clear. Here, we observed that WTAP also went through phase separation both *in vitro* and *in vivo*. We found WTAP mainly formed the aggregates with lower mobility in untreated cells, and transited to liquid droplets with IFN-β treatment,

implying that phase separation participated in WTAP-dependent m^6A deposition under IFN-β stimulation. By hex treatment and mutation assay to block phase transition of WTAP, we confirmed that low mobility of WTAP aggregates restricted the binding affinity to ISGs promoter region and inhibited the m^6A deposition, while IFN-β-induced phase transition of WTAP resulted in the higher binding affinity and m^6A modification level on ISGs mRNA. These results demonstrated the mechanism and the crucial role of WTAP phase separation and phase transition in MTC assembly and ISGs m^6A deposition under IFN-β stimulation. Furthermore, the phase transition of WTAP suggested a potential mechanism that aggregation of WTAP might work as a backup storage, and the stimuli-induced phase transition was developed to perform the m^6A modification timely and precisely in response to the requirement of cell development or abnormal situations. Thus, investigation of WTAP phase separation in different model could be conducted to explain the mechanism of m^6A modification under different stimulation and explore possible therapeutic targets of multiple diseases.

Post-translational modifications are one of the most common ways to modulate characteristic of proteins (Luo, Wu, & Li, 2021), like phosphorylation of serine and threonine (Markevich, Hoek, & Kholodenko, 2004), methylation of arginine (Guccione & Richard, 2019). Several reports indicated that phosphorylation of phase-separated proteins are associated with the solid/gel-like aggregates formation or solid/gel-to-liquid phase transition, participating in various physiological process such as the pathogenesis of tau protein aggregates or acute transcriptional response (Arendt, Stieler, & Holzer, 2016; Boyko et al., 2019; H. Zhang et al., 2022), but whether the phosphorylation-controlled phase transition of proteins regulated other physiological process remains to be illustrated. In this study, we observed that phosphorylation of WTAP promoted the aggregates formation with lower mobility of WTAP, while IFN-β induced the dephosphorylation of WTAP by PPP4 at multiple serine sites, led to the gel-to-liquid phase transition of WTAP. Consistently, phosphomimic 5ST-D mutant of WTAP mainly aggregated as lower mobility form compared to phosphodeficient 5ST-A mutant of WTAP, which formed liquid droplets

in cells, indicating that phosphorylation level of WTAP balanced its phase transition. Therefore, our findings shed light on the mechanism of post-translational modification-regulated phase transition of WTAP and put forward an open question whether phosphorylation and other post-translational modifications function as the key strategy for global phase transition of proteins *in vivo*.

As a global modification in cells, m^6A modification could be hindered by MTC along with the inhibition role of exon junction complex, led to the specificity of modification, mapping the m^6A topology and maintain in stable state (He et al., 2023; Uzonyi et al., 2023). More and more results suggesting that MTC could be recruited and enriched in different chromatin loci, including promoter or enhancer, to dynamically deposit m^6A modification on nascent mRNA co-transcriptionally under certain circumstance or function in various physiological activities, implying the importance of interaction between MTC and chromatin architecture (Dou et al., 2023; Sendinc & Shi, 2023; Xu et al., 2022). In this work, we validated the IFN-β-induced STAT1-WTAP-METTL3 interaction guiding MTC to the promoter region of ISGs to direct the m^6A modification on ISGs mRNA and regulate the mRNA decay. Similarly, Bertero *et al* found that TGF-β-activated transcriptional factor SMAD2/3 recruits MTC and specifically directed the m^6A modification and degradation of a subset of downstream transcripts, which affects the early cell fate decision (Bertero et al., 2018). These studies uncovered the mechanism of phase transition-mediated transcriptional factor-MTC interaction directed m^6A modification of downstream genes co-transcriptionally in maintaining the cellular homeostasis under specific stimulation, raised a new perspective on the cooperation of gene transcription and mRNA modification.

Taken together, our study drew a full picture of the phase transition behavior of WTAP and the function of STAT1-WTAP-MTC directed m^6A modification on ISGs mRNA under IFN-β stimulation. Our findings unraveled a novel mechanism of finetuning m^6A methylated mRNA profile under stimulation, and provided a possible therapeutic target in antiviral responses and many other diseases.

Materials and Methods

Cells.

THP-1 cells obtained from the Cell Bank of the Chinese Academy of Sciences (Shanghai, China) were cultured in RPMI 1640 (Gibco) with 10% (vol/vol) fetal bovine serum (FBS), 1% penicillin-streptomycin (Gibco,1:100) and 1% L-glutamine (Gibco) incubated in a 37°C chamber with 5% CO_2 (Thermo Fisher Scientific). Before stimulation, THP-1 cells were differentiated into macrophages (THP-1-deirived macrophages) through treatment of 100 nM phorbol-12-myristate-13-acetate (PMA) (P8139, Sigma) for 16 hours. After PMA treatment, the macrophages were rested for 48 hours before stimulation. A549 and HeLa cells obtained from the Cell Bank of the Chinese Academy of Sciences (Shanghai, China) were cultured in DMEM medium (Corning) with 10% FBS and 1% L-glutamine (Gibco) incubated in a 37°C chamber with 5% CO_2.

Reagents and Antibodies.

IFN-β (cat. #300-02BC) was purchased from PeproTech Inc. PMA (cat. #P1585), puromycin (cat. #P9620), Actinomycin D (cat. #SBR00013), 1,6-hexanediol (cat. #240117), digitonin (cat. #D141), DTT (cat. #3483-12-3), DAPI (cat. #D9542) were purchased from Sigma-Aldrich. Isopropyl-beta-D-thiogalactopyranoside (IPTG, cat. #CA413) and Superluminal™ High- efficiency Transfection Reagent (cat. # 11231804) were purchased from MIKX. NP-40 (cat. #P0013F) was purchased from Beyotime Biotechnology. The antibodies that used in this study were listed in *Table S1*.

Generation of knockout cell lines by CRISPR/Cas9.

After THP-1 cells were seeded, medium was replaced by DMEM containing polybrene (8 μg/ml) (Sigma-Aldrich) lentiviral vector encoding Cas9 and small guide RNAs (sgRNA) for 48 hours. Cells were selected using puromycin (Sigma-Aldrich). The sequence of sgRNAs targeting indicated gene obtained from Sangon (Shanghai, China) were listed in *Table S2*:

siRNA Transfection.

siRNA duplexes and scrambled siRNA were chemically synthesized by RIBOBIO (Guangzhou, China) and transfected into cells using LipoRNAiMAX reagent (Invitrogen) according to the manufacturer's instructions. The sequences of siRNAs were listed in *Table S2*:

Virus infection.

VSV and HSV-1 were amplificated and tittered on Vero E6 cell line. Virus titers were measured by means of 50% of the tissue culture's infectious dose (TCID50). Virus were infected into indicated cell lines with indicated titers as shown in figure legends.

Immunoblot (IB) assays and immunoprecipitation (IP).

Relevant cells were stimulated as indicated, and whole cell lysate was obtained using low-salt lysis buffer (50 mM Hepes (pH 7.5), 150 mM NaCl, 1 mM EDTA, 1.5 mM $MgCl_2$, 10% glycerol, 1% Triton X-100, supplemented with protease inhibitor cocktail (cat. #A32965, Pierce) and phosSTOP Phosphatase Inhibitor Cocktail (cat. #4906837001, Roche)). Cell lysates were centrifuged at 4°C, 12000 g for 15 minutes and supernatants was boiled at 100 °C for 5 minutes with the 5×Loading Buffer (cat. #FD006, Hangzhou Fude Biological Technology Co, LTD.). Solution was resolved by SDS-PAGE, transferred to polyvinylidene fluoride (PVDF) membranes (cat. #1620177, Bio-Rad Laboratories, Inc.), blocked with 5% skim milk (cat. #232100, BD) for 1 hour and incubated with appropriate antibody. Immobilon Western HRP Substrate (cat. #WBKLS0500, Millipore) was used for protein detection with ChemiDoc MP System (Bio-Rad Laboratories, Inc.) and Image Lab version 6.0 (Bio-Rad software, California, USA). For immunoprecipitation, protein samples were incubated with protein A/G beads (cat. #20333, #20399, Pierce) or anti-Flag M2 affinity gel (cat. #A2220, Sigma-Aldrich) together with indicated antibody at 4°C overnight. Beads were washed five times with low-salt lysis buffer and boiled at 100 °C for 5 minutes with 2×SDS loading buffer, followed with immunoblot assays

described above.

Mass spectrometry.

HEK 293T cells were transfected with plasmids expressing mCherry-WTAP. 24 hours after transfection, whole cell lysate was obtained using low-salt lysis buffer and immunoprecipitated using protein A/G beads together with anti-WTAP antibody at 4°C overnight. Proteins were obtained from beads and analyzed by LC-MS/MS analysis. Details were shown in *SI Appendix, Extended Methods*.

RNA extraction, quantitative real-time polymerase chain reaction (qPCR) and RNA sequencing (RNA-Seq) assay.

Relevant cells were treated as indicated and total RNA was extracted from cells with TRIzol reagent (cat. #15596026, Invitrogen), according to the manufacturer's instructions. RNA was then reverse-transcribed into cDNA using HiScript® III RT SuperMix for qPCR (+gDNA wiper) (cat. #R323-01, Vazyme). The level of indicated genes were determined by qPCR with 2×PolarSignal™ SYBR Green mix Taq (cat. #MKG900-10, MIKX) using LightCycler® 480 System (Roche). The primers used in qPCR were listed in Table S2. For RNA-Seq assay, total RNA was isolated from cells using TRIzol reagent, and sequencing was performed by Sangon Biotech (Shanghai, China). Details of RNA-Seq data analysis were shown in *SI Appendix, Extended Methods*.

Chromatin-immunoprecipitation (ChIP) assay.

THP-1 cells were treated as indicated and DNA were enriched through ChIP assay referred to the Rockland Chromatin Immunoprecipitation assay protocol. Details were shown in *SI Appendix, Extended Methods*. After ChIP enrichment, DNA were analyzed through qPCR assay. The sequences of primers were listed in *Table S2*:

RNA-immunoprecipitation (RIP) followed with qPCR assay.

THP-1 cells were treated as indicated and RNA were enriched through RIP assay

referred to the previously reported protocol (Keene, Komisarow, & Friedersdorf, 2006). Details were shown in *SI Appendix, Extended Methods*. After RIP enrichment, RNA were analyzed through qPCR assay. The sequences of primers were listed in *Table S2*:

m^6A methylated RNA immunoprecipitation (MeRIP) followed with qPCR assay and MeRIP-Seq assay.

For MeRIP-qPCR, the procedures were referred to the protocol as manufacturer's instructions. Approximately 2×10^7 cells were seeded and stimulated by 10 ng/mL IFN-β for 6 hours. Approximately more than 50 μg of total RNA was subjected to isolate poly (A) mRNA with poly-T oligo attached magnetic beads (cat. #61006, Invitrogen). Following purification, the poly(A) mRNA fractions is fragmented into ~100-nt-long oligonucleotides using divalent cations under elevated temperature. Then the cleaved RNA fragments were subjected to incubation for 2h at 4°C with m^6A-specific antibody (cat. #202003, Synaptic Systems) in IP buffer (50 mM Tris-HCl, 750 mM NaCl and 0.5% Igepal CA-630) supplemented with BSA (0.5 μg/μL). The mixture was then incubated with protein-A beads and eluted with elution buffer (1×IP buffer and 6.7mM m^6A), while 10% of fragmented mRNA was kept as input. After immunoprecipitation, precipitates were washed by IP buffer for 5 times and RNA was isolated by adding TRIzol reagent. Purified m^6A-containing mRNA fragments and untreated mRNA input control fragments are converted to final cDNA library in accordance with a strand-specific library preparation by dUTP method, and analyzed by qPCR assay. The primers used in qPCR were listed in Table S2.

For MeRIP-Seq, approximately 5×10^7 cells were seeded and stimulated by 10 ng/mL IFN-β for 4 hours. After stimulation, total RNA was extracted using TRIzol reagent. The total RNA quality and quantity were analysis of Bioanalyzer 2100 and RNA 6000 Nano LabChip Kit (Agilent, CA, USA) with RIN number >7.0, followed with MeRIP assay. And then we performed the paired-end 2×150 bp sequencing on an Illumina Novaseq 6000 platform at the LC-BIO Bio-tech ltd (Hangzhou, China) following the vendor's recommended protocol. Details of MeRIP-Seq data analysis

were shown in *SI Appendix, Extended Methods*.

Immunofluorescence staining (IF) and imaging.

THP-1-derived macrophages were differentiated and stimulated as described above. After stimulation, cells were fixed by in 4% paraformaldehyde (Meilunbio, China) for 15 minutes at room temperature, permeated by ice-cold methanol at -20 °C for 15 minutes and blocked using 6% goat serum (cat. #AR1009, Boster Biological) for 1 hour, and then incubated with indicated primary antibody at 4°C overnight, followed by incubation with indicated secondary antibody at room temperature for 1 hour. Phosphate buffer (PBS) was used to wash three times for 5 minutes between each step. After staining, Leica TCS-SP8 STED 3X confocal fluorescence microscope was used to acquire images. Images were captured by Leica TCS-SP8 STED 3X confocal fluorescence microscope and analyzed by Leica Application Suite Advanced Fluorescence (LAS AF, Version 4.2) software, while deconvolution was conducted by Huygens Software (Version 23.04). The colocalization between proteins was quantified by ImageJ software (National Institutes of Health, Maryland, USA, Version 1.52) using Pearson's correlation coefficient, ranging from -1 to 1. A value of -1 represents perfect negative correlation, 0 means no correlation and 1 indicates perfect correlation.

Expression, purification, and interaction of mCherry-WTAP WT, 5ST-A/ST-D mutants, CFP-METTL3 and GFP-STAT1.

Procedures of the expression of proteins in *E.* coli were referred to Hao Jiang et al(H. Jiang et al., 2015). Recombinant mCherry-WTAP, CFP-METTL3 and GFP-STAT1 were cloned into pET-28A plasmid, while ST-D and 5ST-A mutants of WTAP were constructed by mutating the pET-28A-mCherry-WTAP plasmid using Muta-direct^{TM} Kit (Sbsgene, cat. #SDM-15). After transformed into *E.* coli, protein was extracted as shown in *SI Appendix, Extended Methods*.

For detection of interaction among mCherry-WTAP or its indicated mutants, CFP-METTL3 and GFP-STAT, purified proteins were mixed using physiological buffer (20

mM Tris-HCl, pH 7.5, 150 mM KCl, 10% PEG8000) in the final concentration of 10 μM and placed on the slides. Mixtures were incubated and imaged at 37°C in a live-cell-imaging chamber of Leica TCS-SP8 STED 3X confocal fluorescence microscope while images were analyzed by LAS AF software.

Phase separation assay and fluorescence recovery after photobleaching (FRAP). Expression, purification, and interaction of mCherry-WTAP WT, 5ST-A/ST-D mutants, CFP-METTL3 and GFP-STAT1 were shown in *SI Appendix, Extended Methods*. For *in vitro* phase separation assay, recombinant mCherry-WTAP WT, NTD, CTD, ΔPLD, 5ST-D and 5ST-A mutants in indicated concentration were mixed with physiological buffer (20 mM Tris-HCl, pH 7.5, 150 mM KCl, 10% PEG8000). After incubation, turbid solution in the 200 μL PCR tubes were directed observed. For further capture of fluorescence images, solution of recombinant mCherry-WTAP and physiological buffer were treated with or without hex at a final concentration of 10% and placed on dishes. Leica TCS-SP8 STED 3X confocal fluorescence microscope with live-cell-imaging chamber at 37°C was used to capture fluorescence images and the 3D images. For in cells separation assay, plasmids expression mCherry-WTAP WT, 5ST-D and 5ST-A were transfected into HeLa cells for 24 hours, and treated with or without 5% hex and 20 μg/mL digitonin for 1 hour. Leica TCS-SP8 STED 3X confocal fluorescence microscope with live-cell-imaging chamber at 37°C was used to capture fluorescence images. For observing the fusion of condensates, recombinant mCherry-WTAP mixed with physiological buffer or HeLa cells transfected with mCherry-WTAP plasmids were incubated in the live-cell-imaging chamber at 37°C and. Images were captured by Leica TCS-SP8 STED 3X confocal fluorescence microscope, while deconvolution was conducted by Huygens software.

For *in vitro* FRAP experiments were performed on Leica TCS-SP8 STED 3X confocal fluorescence microscope. Recombinant mCherry-WTAP WT, NTD, CTD, 5ST-D and 5ST-A mutants in indicated concentration was mixed with physiological buffer on dishes. For in cells FRAP experiment, HeLa cells transfected with mCherry-WTAP WT, 5ST-D and 5ST-A mutants were treated as indicated. Samples were

imaged with Leica TCS-SP8 STED 3X confocal fluorescence microscope with live-cell-imaging chamber at 37°C. Spots of mCherry-WTAP foci were photobleached with 100% laser power using 567-nm lasers followed with time-lapse images. Images were analyzed by LAS AF software. Fluorescence intensities of regions of interest (ROIs) were corrected by unbleached control regions and then normalized to pre-bleached intensities of the ROIs.

Statistical Analysis.

The data of all quantitative experiments are represented as mean ± SEM of three independent experiments. Statistical analyses were performed with GraphPad Prism software version 8.0 (GraphPad software, California, USA) using two-way analysis of variance (ANOVA) followed by Tukey's test or unpaired two-tailed Student's *t*-test as described in the figure legends. P-value < 0.05 was considered as statistically significant of all statistical analyses.

Data availability.

Raw data of RNA-Seq and MeRIP-Seq have been deposited in the Sequence Read Archive (SRA) database under accession code PRJNA680033 and PRJNA680974, respectively. The data that support this study are available within the article and its Supplementary Information files or available from the authors upon request.

Acknowledgements This work was supported by the National Key R&D Program of China (2020YFA0908700), National Natural Science Foundation of China (92042303, 31870862, 31970700), and Guangdong Basic and Applied Basic Research Foundation (2020B1515120090).

Author Contributions: *J.C.* conceived the project. *J.C.*, *S.C.* and *J.Z.* designed the experiments. *S.C.*, *J.Z.* and *S.J.* expressed and purified the proteins using *E. coli* system while *S.C.*, *J.Z.* and C.Z. finished the rest of the experiments. *X.L.*, *J.R.*, *S.C.*

and *J.Z.* analyzed the data of RNA-Seq and MeRIP-Seq. All authors discussed the results and commented on or prepared the manuscript.

Competing Interest: The authors declare no competing interests.

References

Alberti, S., Gladfelter, A., & Mittag, T. (2019). Considerations and Challenges in Studying Liquid-Liquid Phase Separation and Biomolecular Condensates. *Cell, 176*(3), 419-434. doi:10.1016/j.cell.2018.12.035

Arendt, T., Stieler, J. T., & Holzer, M. (2016). Tau and tauopathies. *Brain Res Bull, 126*(Pt 3), 238-292. doi:10.1016/j.brainresbull.2016.08.018

Bertero, A., Brown, S., Madrigal, P., Osnato, A., Ortmann, D., Yiangou, L., . . . Vallier, L. (2018). The SMAD2/3 interactome reveals that TGFβ controls m6A mRNA methylation in pluripotency. *Nature, 555*(7695), 256-259. doi:10.1038/nature25784

Boyko, S., Qi, X., Chen, T. H., Surewicz, K., & Surewicz, W. K. (2019). Liquid-liquid phase separation of tau protein: The crucial role of electrostatic interactions. *J Biol Chem, 294*(29), 11054-11059. doi:10.1074/jbc.AC119.009198

Chen, Y., Peng, C., Chen, J., Chen, D., Yang, B., He, B., . . . Zheng, S. (2019). WTAP facilitates progression of hepatocellular carcinoma via m6A-HuR-dependent epigenetic silencing of ETS1. *Mol Cancer, 18*(1), 127. doi:10.1186/s12943-019-1053-8

Cho, S., Lee, G., Pickering, B. F., Jang, C., Park, J. H., He, L., . . . Blenis, J. (2021). mTORC1 promotes cell growth via m^6A-dependent mRNA degradation. *Mol Cell, 81*(10), 2064-2075 e2068. doi:10.1016/j.molcel.2021.03.010

Cui, J., Song, Y., Li, Y., Zhu, Q., Tan, P., Qin, Y., . . . Wang, R. F. (2014). USP3 inhibits type I interferon signaling by deubiquitinating RIG-I-like receptors. *Cell Res, 24*(4), 400-416. doi:10.1038/cr.2013.170

Dou, X., Xiao, Y., Shen, C., Wang, K., Wu, T., Liu, C., . . . He, C. (2023). RBFOX2 recognizes N(6)-methyladenosine to suppress transcription and block myeloid leukaemia differentiation. *Nat Cell Biol, 25*(9), 1359-1368. doi:10.1038/s41556-023-01213-w

Gabryelczyk, B., Cai, H., Shi, X., Sun, Y., Swinkels, P. J. M., Salentinig, S., . . . Miserez, A. (2019). Hydrogen bond guidance and aromatic stacking drive liquid-liquid phase separation of intrinsically disordered histidine-rich peptides. *Nat Commun, 10*(1), 5465. doi:10.1038/s41467-019-13469-8

Gao, Y., Pei, G., Li, D., Li, R., Shao, Y., Zhang, Q. C., & Li, P. (2019). Multivalent m^6A motifs promote phase separation of YTHDF proteins. *Cell Res, 29*(9), 767-769. doi:10.1038/s41422-019-0210-3

Garcias Morales, D., & Reyes, J. L. (2021). A birds'-eye view of the activity and specificity of the mRNA m^6A methyltransferase complex. *Wiley Interdiscip Rev RNA, 12*(1), e1618. doi:10.1002/wrna.1618

Geula, S., Moshitch-Moshkovitz, S., Dominissini, D., Mansour, A. A., Kol, N., Salmon-Divon, M., . . . Hanna, J. H. (2015). Stem cells. m6A mRNA methylation facilitates resolution of naive pluripotency toward differentiation. *Science, 347*(6225), 1002-1006. doi:10.1126/science.1261417

Goubau, D., Deddouche, S., & Reis e Sousa, C. (2013). Cytosolic sensing of viruses. *Immunity, 38*(5), 855-869. doi:10.1016/j.immuni.2013.05.007

Gourfinkel-An, I., Cancel, G., Trottier, Y., Devys, D., Tora, L., Lutz, Y., . . . Hirsch, E. C. (1997). Differential distribution of the normal and mutated forms of huntingtin in the human brain. *Ann Neurol, 42*(5), 712-719. doi:10.1002/ana.410420507

Guccione, E., & Richard, S. (2019). The regulation, functions and clinical relevance of arginine methylation. *Nat Rev Mol Cell Biol, 20*(10), 642-657. doi:10.1038/s41580-019-0155-x

Han, D., Longhini, A. P., Zhang, X., Hoang, V., Wilson, M. Z., & Kosik, K. S. (2022). Dynamic assembly of the mRNA m6A methyltransferase complex is

regulated by METTL3 phase separation. *PLoS Biol, 20*(2), e3001535. doi:10.1371/journal.pbio.3001535

He, P. C., Wei, J., Dou, X., Harada, B. T., Zhang, Z., Ge, R., . . . He, C. (2023). Exon architecture controls mRNA m(6)A suppression and gene expression. *Science, 379*(6633), 677-682. doi:10.1126/science.abj9090

Henault, J., Riggs, J. M., Karnell, J. L., Liarski, V. M., Li, J., Shirinian, L., . . . Sanjuan, M. A. (2016). Self-reactive IgE exacerbates interferon responses associated with autoimmunity. *Nat Immunol, 17*(2), 196-203. doi:10.1038/ni.3326

Hu, H., Miao, Y. R., Jia, L. H., Yu, Q. Y., Zhang, Q., & Guo, A. Y. (2019). AnimalTFDB 3.0: a comprehensive resource for annotation and prediction of animal transcription factors. *Nucleic Acids Res, 47*(D1), D33-D38. doi:10.1093/nar/gky822

Huang, Q., Mo, J., Liao, Z., Chen, X., & Zhang, B. (2022). The RNA m^6A writer WTAP in diseases: structure, roles, and mechanisms. *Cell Death Dis, 13*(10), 852. doi:10.1038/s41419-022-05268-9

Jia, G., Fu, Y., Zhao, X., Dai, Q., Zheng, G., Yang, Y., . . . He, C. (2011). N6-Methyladenosine in nuclear RNA is a major substrate of the obesity-associated FTO. *Nature Chemical Biology, 7*(12), 885-887. doi:10.1038/nchembio.687

Jiang, H., Wang, S., Huang, Y., He, X., Cui, H., Zhu, X., & Zheng, Y. (2015). Phase transition of spindle-associated protein regulate spindle apparatus assembly. *Cell, 163*(1), 108-122. doi:10.1016/j.cell.2015.08.010

Jiang, X., Liu, B., Nie, Z., Duan, L., Xiong, Q., Jin, Z., . . . Chen, Y. (2021). The role of m6A modification in the biological functions and diseases. *Signal Transduct Target Ther, 6*(1), 74. doi:10.1038/s41392-020-00450-x

Keene, J. D., Komisarow, J. M., & Friedersdorf, M. B. (2006). RIP-Chip: the isolation and identification of mRNAs, microRNAs and protein components of ribonucleoprotein complexes from cell extracts. *Nat Protoc, 1*(1), 302-307. doi:10.1038/nprot.2006.47

Knuckles, P., & Bühler, M. (2018). Adenosine methylation as a molecular imprint defining the fate of RNA. *FEBS Letters, 592*(17), 2845-2859. doi:10.1002/1873-3468.13107

Lee, J. H., Wang, R., Xiong, F., Krakowiak, J., Liao, Z., Nguyen, P. T., . . . Li, W. (2021). Enhancer RNA m6A methylation facilitates transcriptional condensate formation and gene activation. *Mol Cell, 81*(16), 3368-3385 e3369. doi:10.1016/j.molcel.2021.07.024

Li, J., Chen, K., Dong, X., Xu, Y., Sun, Q., Wang, H., . . . Luo, M. (2022). YTHDF1 promotes mRNA degradation via YTHDF1-AGO2 interaction and phase separation. *Cell Prolif, 55*(1), e13157. doi:10.1111/cpr.13157

Li, Z. X., Zheng, Z. Q., Yang, P. Y., Lin, L., Zhou, G. Q., Lv, J. W., . . . Sun, Y. (2022). WTAP-mediated m^6A modification of lncRNA DIAPH1-AS1 enhances its stability to facilitate nasopharyngeal carcinoma growth and metastasis. *Cell Death Differ, 29*(6), 1137-1151. doi:10.1038/s41418-021-00905-w

Luo, Y. Y., Wu, J. J., & Li, Y. M. (2021). Regulation of liquid-liquid phase separation with focus on post-translational modifications. *Chem Commun (Camb), 57*(98), 13275-13287. doi:10.1039/d1cc05266g

Markevich, N. I., Hoek, J. B., & Kholodenko, B. N. (2004). Signaling switches and bistability arising from multisite phosphorylation in protein kinase cascades. *J Cell Biol, 164*(3), 353-359. doi:10.1083/jcb.200308060

McFadden, M. J., McIntyre, A. B. R., Mourelatos, H., Abell, N. S., Gokhale, N. S., Ipas, H., . . . Horner, S. M. (2021). Post-transcriptional regulation of antiviral gene expression by N6-methyladenosine. *Cell Rep, 34*(9), 108798. doi:10.1016/j.celrep.2021.108798

Meyer, K. D., & Jaffrey, S. R. (2017). Rethinking m^6A Readers, Writers, and Erasers. *Annu Rev Cell Dev Biol, 33*, 319-342. doi:10.1146/annurev-cellbio-100616-060758

Mowen, K. A., Tang, J., Zhu, W., Schurter, B. T., Shuai, K., Herschman, H. R., & David, M. (2001). Arginine methylation of STAT1 modulates IFNalpha/beta-

induced transcription. *Cell, 104*(5), 731-741. doi:10.1016/s0092-8674(01)00269-0

Murthy, A. C., Dignon, G. L., Kan, Y., Zerze, G. H., Parekh, S. H., Mittal, J., & Fawzi, N. L. (2019). Molecular interactions underlying liquid-liquid phase separation of the FUS low-complexity domain. *Nat Struct Mol Biol, 26*(7), 637-648. doi:10.1038/s41594-019-0250-x

Oerum, S., Meynier, V., Catala, M., & Tisne, C. (2021). A comprehensive review of m6A/m6Am RNA methyltransferase structures. *Nucleic Acids Res, 49*(13), 7239-7255. doi:10.1093/nar/gkab378

Perutz, M. F. (1996). Glutamine repeats and inherited neurodegenerative diseases: molecular aspects. *Curr Opin Struct Biol, 6*(6), 848-858. doi:10.1016/s0959-440x(96)80016-9

Qin, Y., Liu, Q., Tian, S., Xie, W., Cui, J., & Wang, R. F. (2016). TRIM9 short isoform preferentially promotes DNA and RNA virus-induced production of type I interferon by recruiting GSK3beta to TBK1. *Cell Res, 26*(5), 613-628. doi:10.1038/cr.2016.27

Reichheld, S. E., Muiznieks, L. D., Keeley, F. W., & Sharpe, S. (2017). Direct observation of structure and dynamics during phase separation of an elastomeric protein. *Proc Natl Acad Sci U S A, 114*(22), E4408-E4415. doi:10.1073/pnas.1701877114

Ries, R. J., Zaccara, S., Klein, P., Olarerin-George, A., Namkoong, S., Pickering, B. F., . . . Jaffrey, S. R. (2019). m^6A enhances the phase separation potential of mRNA. *Nature, 571*(7765), 424-428. doi:10.1038/s41586-019-1374-1

Rubio, R. M., Depledge, D. P., Bianco, C., Thompson, L., & Mohr, I. (2018). RNA m^6A modification enzymes shape innate responses to DNA by regulating interferon beta. *Genes Dev, 32*(23-24), 1472-1484. doi:10.1101/gad.319475.118

Schapira, M. (2016). Structural Chemistry of Human RNA Methyltransferases. *ACS Chem Biol, 11*(3), 575-582. doi:10.1021/acschembio.5b00781

Schneider, W. M., Chevillotte, M. D., & Rice, C. M. (2014). Interferon-stimulated genes: a complex web of host defenses. *Annu Rev Immunol, 32*, 513-545. doi:10.1146/annurev-immunol-032713-120231

Sendinc, E., & Shi, Y. (2023). RNA m6A methylation across the transcriptome. *Mol Cell, 83*(3), 428-441. doi:10.1016/j.molcel.2023.01.006

Shi, H., Wang, X., Lu, Z., Zhao, B. S., Ma, H., Hsu, P. J., . . . He, C. (2017). YTHDF3 facilitates translation and decay of N(6)-methyladenosine-modified RNA. *Cell Res, 27*(3), 315-328. doi:10.1038/cr.2017.15

Tanaka, M., Morishima, I., Akagi, T., Hashikawa, T., & Nukina, N. (2001). Intra- and intermolecular beta-pleated sheet formation in glutamine-repeat inserted myoglobin as a model for polyglutamine diseases. *J Biol Chem, 276*(48), 45470-45475. doi:10.1074/jbc.M107502200

Uddin, S., Sassano, A., Deb, D. K., Verma, A., Majchrzak, B., Rahman, A., . . . Platanias, L. C. (2002). Protein kinase C-delta (PKC-delta) is activated by type I interferons and mediates phosphorylation of Stat1 on serine 727. *Journal Of Biological Chemistry, 277*(17), 14408-14416. doi:10.1074/jbc.M109671200

Uzonyi, A., Dierks, D., Nir, R., Kwon, O. S., Toth, U., Barbosa, I., . . . Schwartz, S. (2023). Exclusion of m6A from splice-site proximal regions by the exon junction complex dictates m6A topologies and mRNA stability. *Mol Cell, 83*(2), 237-251 e237. doi:10.1016/j.molcel.2022.12.026

Wang, J., Choi, J.-M., Holehouse, A. S., Lee, H. O., Zhang, X., Jahnel, M., . . . Hyman, A. A. (2018). A Molecular Grammar Governing the Driving Forces for Phase Separation of Prion-like RNA Binding Proteins. *Cell, 174*(3), 688-699.e616. doi:10.1016/j.cell.2018.06.006

Wang, J., Wang, L., Diao, J., Shi, Y. G., Shi, Y., Ma, H., & Shen, H. (2020). Binding to m^6A RNA promotes YTHDF2-mediated phase separation. *Protein Cell, 11*(4), 304-307. doi:10.1007/s13238-019-00660-2

Wang, L., Hui, H., Agrawal, K., Kang, Y., Li, N., Tang, R., . . . Rana, T. M. (2020). m^6A RNA methyltransferases METTL3/14 regulate immune responses to anti-PD-1 therapy. *EMBO J, 39*(20), e104514. doi:10.15252/embj.2020104514

Wang, X., Lu, Z., Gomez, A., Hon, G. C., Yue, Y., Han, D., . . . He, C. (2014). N6-methyladenosine-dependent regulation of messenger RNA stability. *Nature, 505*(7481), 117-120. doi:10.1038/nature12730

Wang, X., Zhao, B. S., Roundtree, I. A., Lu, Z., Han, D., Ma, H., . . . He, C. (2015). N(6)-methyladenosine Modulates Messenger RNA Translation Efficiency. *Cell, 161*(6), 1388-1399. doi:10.1016/j.cell.2015.05.014

Wen Z, Zhong Z, & Jr., D. J. (1995). Maximal activation of transcription by Stat1 and Stat3 requires both tyrosine and serine phosphorylation. *Cell, 82*(2), 241-250. doi:10.1016/0092-8674(95)90311-9

Winkler, R., Gillis, E., Lasman, L., Safra, M., Geula, S., Soyris, C., . . . Stern-Ginossar, N. (2019). m^6A modification controls the innate immune response to infection by targeting type I interferons. *Nat Immunol, 20*(2), 173-182. doi:10.1038/s41590-018-0275-z

Xu, W., He, C., Kaye, E. G., Li, J., Mu, M., Nelson, G. M., . . . Shen, H. (2022). Dynamic control of chromatin-associated m(6)A methylation regulates nascent RNA synthesis. *Mol Cell, 82*(6), 1156-1168 e1157. doi:10.1016/j.molcel.2022.02.006

Yu, H., Zhao, K., Zeng, H., Li, Z., Chen, K., Zhang, Z., . . . Wu, Z. (2021). N^6-methyladenosine (m^6A) methyltransferase WTAP accelerates the Warburg effect of gastric cancer through regulating HK2 stability. *Biomed Pharmacother, 133*, 111075. doi:10.1016/j.biopha.2020.111075

Zhang, H., Shao, S., Zeng, Y., Wang, X., Qin, Y., Ren, Q., . . . Sun, Y. (2022). Reversible phase separation of HSF1 is required for an acute transcriptional response during heat shock. *Nat Cell Biol, 24*(3), 340-352. doi:10.1038/s41556-022-00846-7

Zhang, Z., Theler, D., Kaminska, K. H., Hiller, M., de la Grange, P., Pudimat, R., . . . Stamm, S. (2010). The YTH domain is a novel RNA binding domain. *J Biol Chem, 285*(19), 14701-14710. doi:10.1074/jbc.M110.104711

Zheng, G., Dahl, J. A., Niu, Y., Fedorcsak, P., Huang, C. M., Li, C. J., . . . He, C. (2013). ALKBH5 is a mammalian RNA demethylase that impacts RNA

metabolism and mouse fertility. *Mol Cell, 49*(1), 18-29. doi:10.1016/j.molcel.2012.10.015

Zhong, X., Yu, J., Frazier, K., Weng, X., Li, Y., Cham, C. M., . . . Leone, V. (2018). Circadian Clock Regulation of Hepatic Lipid Metabolism by Modulation of m^6A mRNA Methylation. *Cell Rep, 25*(7), 1816-1828 e1814. doi:10.1016/j.celrep.2018.10.068

Figure legends

Figure 1 WTAP goes through phase transition with IFN-β stimulation.

(A) THP-1-derived macrophages were infected with VSV (m.o.i. = 0.1) for 24 hours together with or without 5% 1,6-hexanediol (hex) and 10 μg/mL digitonin for 2 hours or left untreated (UT). WTAP (red) were imaged using confocal microscope. from n = 20 cells through ImageJ. Scale bars indicated 5 μm.

(B) HeLa cells were placed on the dishes and stimulated with or without 10 ng/mL IFN-β for 1 hour at 37 °C. After stimulation, endogenous WTAP was stained and imaged using confocal microscopy. The number of WTAP condensates that diameter over 0.4 μm of n = 80 cells were counted while medium with interquartile range was shown. Scale bars indicated 5 μm.

(C) Domain structures (top) and distribution of amino acids (bottom) of WTAP protein. WT, wild type. NTD, N-terminal domain. CTD, C-terminal domain. NLS, nuclear localization signal. PLD, prion-like domain.

(D) Tubes containing physiological buffer with or without recombinant mCherry-WTAP (10 μM) were compared, in which recombinant mCherry-WTAP underwent phase separation.

(E) Foci formation of recombinant mCherry-WTAP (10 μM) with or without 10% 1,6-hexanediol (hex) was observed through confocal microscopy. Scale bars indicated 5 μm.

(F) Phase separation of mCherry-WTAP in mCherry-WTAP-rescued HeLa cells treated with or without 5% 1,6-hexanediol (hex) and 20 μg/mL digitonin were observed through confocal microscopy. Representative images of n=10 cells were shown. Scale bars indicated 10 μm.

(G) mCherry-WTAP-rescued HeLa cells were placed on dishes and treated with or without 10 ng/mL IFN-β for 1 hour at 37 °C. After stimulation, bleaching of the WTAP foci was performed and quantification of FRAP of mCherry-WTAP aggregates was analyzed. The start time point of recovery after photobleaching was defined as 0 second. Representative images of n=10 cells were shown. Scale bars indicated 5 μm.

(H) Recombinant mCherry-WTAP WT, NTD and CTD (40 μM) were mixed with the physiological buffer and placed on the dishes at 37°C (Prebleach). After incubation, bleaching was performed and quantification of fluorescence recovery after photobleaching (FRAP) of recombinant mCherry-WTAP WT, NTD and CTD were analyzed. Representative images of n=6 condensates were shown, and the normalized intensity was measured and analyzed. The start time point of recovery after photobleaching was defined as 0 second. Scale bars indicated 2 μm.

All error bars, mean values ± SD, P-values were determined by unpaired two-tailed Student's *t*-test of n = 20 cells in (A) and n=80 cells in (B). For (A-B and D-H), similar results were obtained for three independent biological experiments.

Figure 2. IFN-β-mediated dephosphorylation of WTAP induces its phase transition.

(A) THP-1-derived macrophages were treated with 10 ng/mL IFN-β for 1 hour or left untreated. Whole cell lysates (WCL) were collected and immunoprecipitation experiment using anti-WTAP antibody or rabbit IgG was performed, followed with immunoblot using anti-phosphoserine/threonine/tyrosine antibody (pan-p). Relative protein level was shown.

(B) THP-1-derived macrophages were treated with 10 ng/mL IFN-β for 1 hour or left untreated. Whole cell lysates (WCL) were collected and immunoprecipitation experiment using anti-WTAP antibody or rabbit IgG was performed, followed with immunoblot.

(C) THP-1-derived macrophages were transfected with scramble (scr) or PPP4-targeted siRNA and stimulated with or without 10 ng/mL IFN-β for 1 hour. WCL were collected and IP experiment with anti-WTAP antibody or rabbit IgG was performed, followed with immunoblot using anti-phosphoserine/threonine/tyrosine antibody (pan-p). Relative protein level was measured and analyzed.

(D) mCherry-WTAP was purified from HEK 293T cells expressing mCherry-WTAP using anti-WTAP antibody and analyzed by mass spectrometry (MS) for the

phosphorylation. Six phosphorylated residues were identified. Data of MS assay for five phosphorylated sites within CTD were shown in Figure 2-figure supplement 1C.

(E-F) Recombinant mCherry-WTAP mutants with indicated Ser/Thr to Asp mutation were listed in (D), while representative images of the phase-separated mCherry-WTAP WT, 5ST-D and 5ST-A mutants were shown in (E). Images of phase separation of other mCherry-WTAP mutants were shown in Figure 2-figure supplement 1D. Scale bars indicated 5 μm.

(G) Recombinant mCherry-WTAP WT (10 μM), 5ST-A mutant (10 μM) or 5ST-D mutant (10 μM) was mixed with the physiological buffer and placed on the dishes at 37°C (Prebleach). After incubation, bleaching was performed and quantification of FRAP of recombinant mCherry-WTAP WT and 5ST-D mutant were analyzed. Representative images of n=5 condensates were shown and the normalized intensity was measured and analyzed. The start time point of recovery after photobleaching was defined as 0 second. Arrow indicated the FRAP area while scale bars indicated 2 μm.

(H) HeLa cells expressing mCherry-WTAP WT, 5ST-D or 5ST-A mutants were placed on the dishes and stimulated with or without 10 ng/mL IFN-β for 1 hour at 37°C. After seeding, bleaching of the WTAP foci was performed and quantification of FRAP of mCherry-WTAP aggregates was analyzed. Representative images of n = 10 cells were shown, and the normalized intensity was measured and analyzed. The start time point of recovery after photobleaching was defined as 0 second. Representative images of n = 10 cells were shown. Scale bars indicated 5 μm.

(I) Schematic figure of phase separation of WTAP WT, 5ST-D and 5ST-A *in vitro* (above) and WTAP WT with IFN-β stimulation or left untreated (UT), 5ST-D and 5ST-A in cells (below).

All error bars, mean values ± SD, P-values were determined by unpaired two-tailed Student's *t*-test of n = 3 independent biological experiments in (A and C). For (A-C and E-H), similar results were obtained for three independent biological experiments.

Figure 3. WTAP phase transition mediates m^{6}A modification to regulate ISG expression.

(A) Transcriptome sequencing analysis of control (*GFP*^{sgRNA}) and *WTAP*^{sgRNA} #2 THP-1-derived macrophages stimulated with 10 ng/mL IFN-β for 0, 6, 12 hours. The count-per-million (CPM) value of the ISGs was drawn by Heatmapper and clustered using Centroid Linkage approach.

(B) Gene ontology analysis for the WTAP down-regulated ISGs.

(C) Transcriptome sequencing analysis of *IFIT1*, *IFIT2*, *OAS1* and *OAS2* in control (*GFP*^{sgRNA}) and *WTAP*^{sgRNA} #2 THP-1-derived macrophages stimulated with 10 ng/mL IFN-β for 4 hours or left untreated (UT).

(D-E) Distribution (D) and topology (E) analysis (5'-UTR, CDS and 3'UTR) of total m^{6}A sites and WTAP-dependent m^{6}A sites.

(F) Control (*GFP*^{sgRNA}) and *WTAP*^{sgRNA} #2 THP-1-derived macrophages were treated with 10 ng/mL IFN-β for 4 hours. MeRIP-qPCR assay of *IFIT1*, *IFIT2*, *OAS1* and *OAS2* was performed and ratios between m^{6}A-modified mRNA and input were shown (m^{6}A IP/input).

(G) Control (*GFP*^{sgRNA}) and *WTAP*^{sgRNA} #2 THP-1-derived macrophages were treated with 10 ng/mL IFN-β together with or without 5% 1,6-hexanediol (hex) and 20 μg/mL digitonin for 2 hours or left untreated. After stimulation, medium was replaced by fresh 1640 medium while total RNA was collected 2 hours later. MeRIP-qPCR analysis of *IFIT1*, *IFIT2*, *OAS1* and *OAS2* was performed and ratios between m^{6}A-modified mRNA and input were shown (m^{6}A IP/input).

(H) THP-1-derived macrophages transfected with scramble (*scr)* siRNA or *PPP4* siRNA were treated with 10 ng/mL IFN-β for 4 hours. MeRIP-qPCR assay of *IFIT1*, *IFIT2*, *OAS1* and *OAS2* was performed and ratios between m^{6}A-modified mRNA and input were shown (m^{6}A IP/input).

(I) Control (*GFP*^{sgRNA}) or *WTAP*^{sgRNA} #2 THP-1-derived macrophages with or without expression of Flag-tagged WTAP WT, and its 5ST-D or 5ST-A mutants were treated with 10 ng/mL IFN-β for 4 hours. MeRIP-qPCR assay of *IFIT1*, *IFIT2*, *OAS1* and

OAS2 was performed and ratios between m^6A-modified mRNA and input were shown (m^6A IP/input).

All error bars, mean values ± SEM, P-values were determined by unpaired two-tailed Student's *t*-test of n=3 independent biological experiments in (F-I).

Figure 4. Liquid-phase separated WTAP bridges STAT1 and m^6A modification methyltransferase complex to direct m^6A modification on ISGs mRNA.

(A) Occupancy of the promoter of the WTAP down-regulated ISGs with lower m^6A level in *WTAP*^{sgRNA} #2 cells (genes were identified in Figure 3A and both -2000-0 bp and -500-0 bp upstream of transcription start site were analyzed) by STAT1, STAT2 and IRF9 was predicted by AnimalTFDB 3.0.

(B) THP-1-derived macrophages were treated with 10 ng/mL IFN-β for indicated time points. Whole cell lysates (WCL) were collected and immunoprecipitation (IP) experiment using anti-STAT1 antibody or rabbit IgG was performed, followed with immunoblot.

(C) Control (*GFP*^{sgRNA}) and *WTAP*^{sgRNA} #2 THP-1-derived macrophages were treated with 10 ng/mL IFN-β for 1 hour or left untreated. WCL were collected and IP experiment using anti-METTL3 antibody or rabbit IgG was performed, followed with immunoblot.

(D) Control (*GFP*^{sgRNA}) and *WTAP*^{sgRNA} #2 THP-1-derived macrophages were treated with 10 ng/mL IFN-β for 2 hour or left untreated. RNA immunoprecipitation (RIP) experiments using anti-METTL3 antibody or rabbit IgG control were performed in control or *WTAP*^{sgRNA} #2 THP-1-derived macrophages treated with 10 ng/mL IFN-β for 2 hours. RNA of *ISGs* enriched by RIP was analyzed by qPCR assay, and the ratios between RIP-enriched RNA and input were shown (RIP enrichment/input).

(E) THP-1-derived macrophages were treated with 10 ng/mL IFN-β for indicated time points together with or without 5% 1,6-hexanediol (hex) and 20 μg/mL digitonin. Whole cell lysates (WCL) were collected and IP experiment with anti-STAT1 antibody or rabbit IgG was performed, followed with immunoblot.

(F) Recombinant GFP-STAT1 (10 μM) and mCherry-WTAP (10 μM) were incubated with or without 10% 1,6-hexanediol (hex). Immunoprecipitation (IP) experiment with anti-STAT1 antibody or rabbit IgG was performed, followed with immunoblot.

(G) THP-1-derived macrophages were treated with 10 ng/mL IFN-β only or with 5% 1,6-hexanediol (hex) and 20 μg/mL digitonin for 1 hour or left UT. Interaction between STAT1 (green) and WTAP (red) were imaged using confocal microscope. Interaction between STAT1 and WTAP determined by Pearson's correlation coefficient was analyzed and calculated from n=80 cells through ImageJ. Scale bars indicated 5 μm.

(H-I) Recombinant GFP-STAT1 (10 μM), mCherry-WTAP (10 μM) and CFP-METTL3 (10 μM) were incubated using physiological buffer at 37°C. After incubation, images were captured using confocal microscope (H). Relative fluorescence intensity of proteins in n=10 condensates were analyzed by ImageJ software (I).

All error bars, mean values ± SEM, P-values were determined by unpaired two-tailed Student's *t*-test of n = 3 independent biological experiments in (D). All error bars, mean values ± SD, P-values were determined by unpaired two-tailed Student's *t*-test of n = 3 independent biological experiments in (I). For (B-D, E-G and H), similar results were obtained for three independent biological experiments.

Figure 5. Phase transition of WTAP mediates its interaction with ISGs promoter region to regulate m^{6}A modification on ISGs mRNA.

(A) Chromatin immunoprecipitation (ChIP) experiments using anti-STAT1 antibody or rabbit IgG control were performed in THP-1-derived macrophages treated with 10 ng/mL IFN-β for 2 hours. Binding between the promoter region of IFIT1, IFIT2, OAS1 and OAS2 with WTAP was detected by qPCR assay and ratios between ChIP-enriched DNA and input were shown (ChIP enrichment/input).

(B) Chromatin immunoprecipitation (ChIP) experiments using anti-WTAP antibody or rabbit IgG control were performed in THP-1-derived macrophages treated with 10

ng/mL IFN-β for 2 hours or left untreated (UT). Binding between the promoters of *IFIT1*, *IFIT2*, *OAS1* and *OAS2* with WTAP were detected by qPCR assay, and the ratios between ChIP-enriched DNA and input were shown (ChIP enrichment/input).

(C) Chromatin immunoprecipitation (ChIP) experiments using anti-WTAP antibody or rabbit IgG control were performed in THP-1-derived macrophages transfected with *scramble* (*scr*) siRNA, *STAT1* siRNA or *PPP4* siRNA treated with 10 ng/mL IFN-β for 2 hours. Binding between the promoter region of *IFIT1*, *IFIT2*, *OAS1* and *OAS2* with WTAP was detected by qPCR assay and ratios between ChIP-enriched DNA and input were shown (ChIP enrichment/input).

(D) ChIP experiments using anti-WTAP antibody or rabbit IgG control were performed in control (GFP^{sgRNA}) or $WTAP^{sgRNA}$ #2 THP-1-derived macrophages with or without expression of Flag-tagged wild type (WT) WTAP, and its 5ST-D or 5ST-A mutants treated with 10 ng/mL IFN-β for 2 hours. Binding between the promoter region of *IFIT1*, *IFIT2*, *OAS1* and *OAS2* with WTAP was detected by qPCR assay and ratios between ChIP-enriched DNA and input were shown (ChIP enrichment/input).

(E) Schematic figure of IFN-β-induced phase transition of WTAP regulates the m^6A modification of ISGs mRNA.

All error bars, mean values ± SEM, P-values were determined by unpaired two-tailed Student's *t*-test of n = 3 independent biological experiments in (A-D).

Figure 1

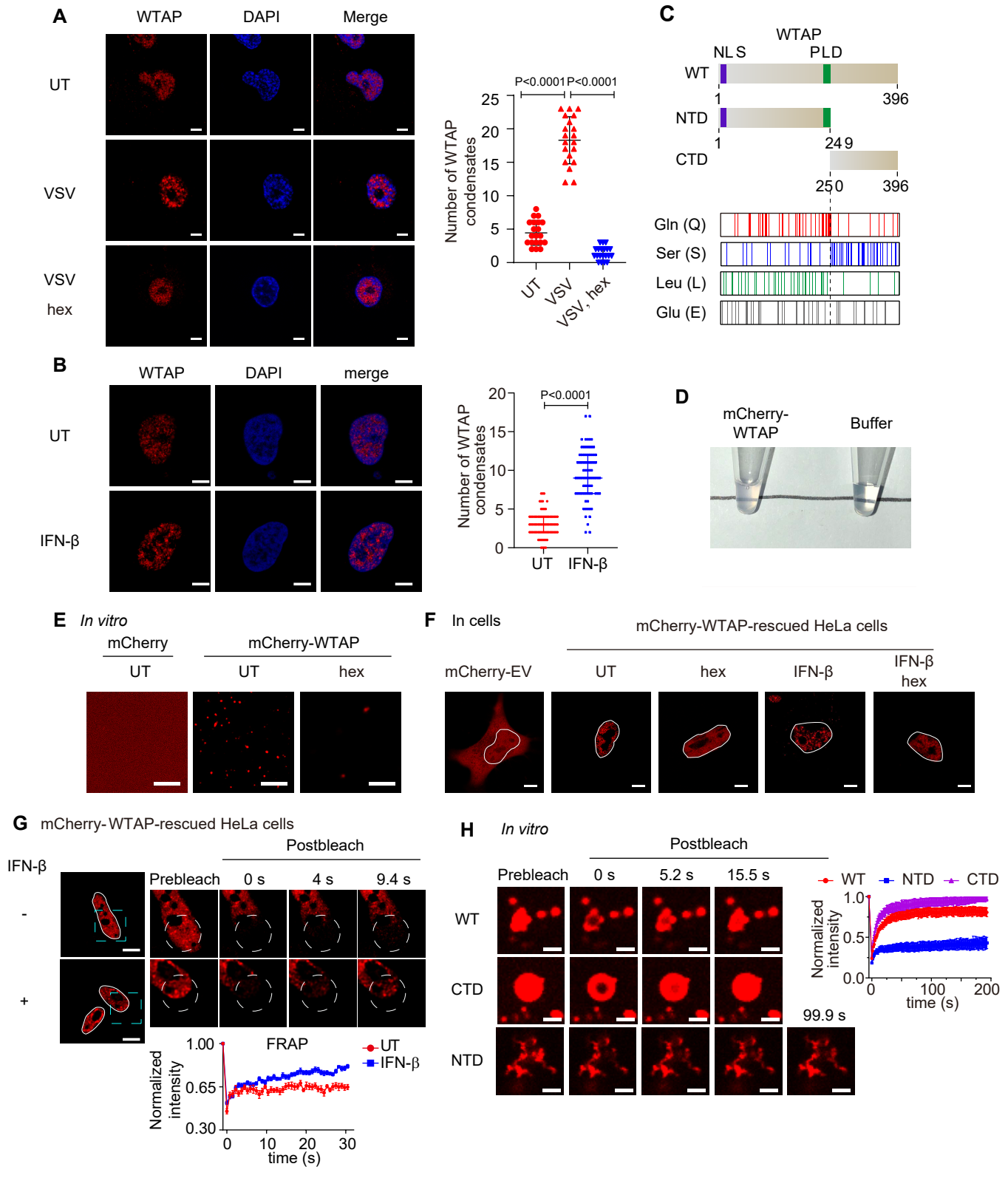
A
WTAP
DAPI
Merge
UT
VSV
VSV hex
P<0.0001
P<0.0001
Number of WTAP condensates
25
20
15
10
5
0
UT
VSV
VSV, hex
C
WTAP
NLS
PLD
WT
1
396
NTD
1
249
CTD
250
396
Gln (Q)
Ser (S)
Leu (L)
Glu (E)
B
WTAP
DAPI
merge
UT
IFN-β
P<0.0001
Number of WTAP condensates
20
15
10
5
0
UT
IFN-β
D
mCherry-WTAP
Buffer
E
In vitro
mCherry
mCherry-WTAP
UT
UT
hex
F
In cells
mCherry-WTAP-rescued HeLa cells
mCherry-EV
UT
hex
IFN-β
IFN-β hex
G
mCherry-WTAP-rescued HeLa cells
Postbleach
IFN-β
-
+
Prebleach
0 s
4 s
9.4 s
FRAP
UT
IFN-β
Normalized intensity
1.00
0.65
0.30
0
10
20
30
time (s)
H
In vitro
Postbleach
Prebleach
0 s
5.2 s
15.5 s
99.9 s
WT
CTD
NTD
WT
NTD
CTD
Normalized intensity
1.0
0.5
0.0
0
100
200
time (s)

Figure 2

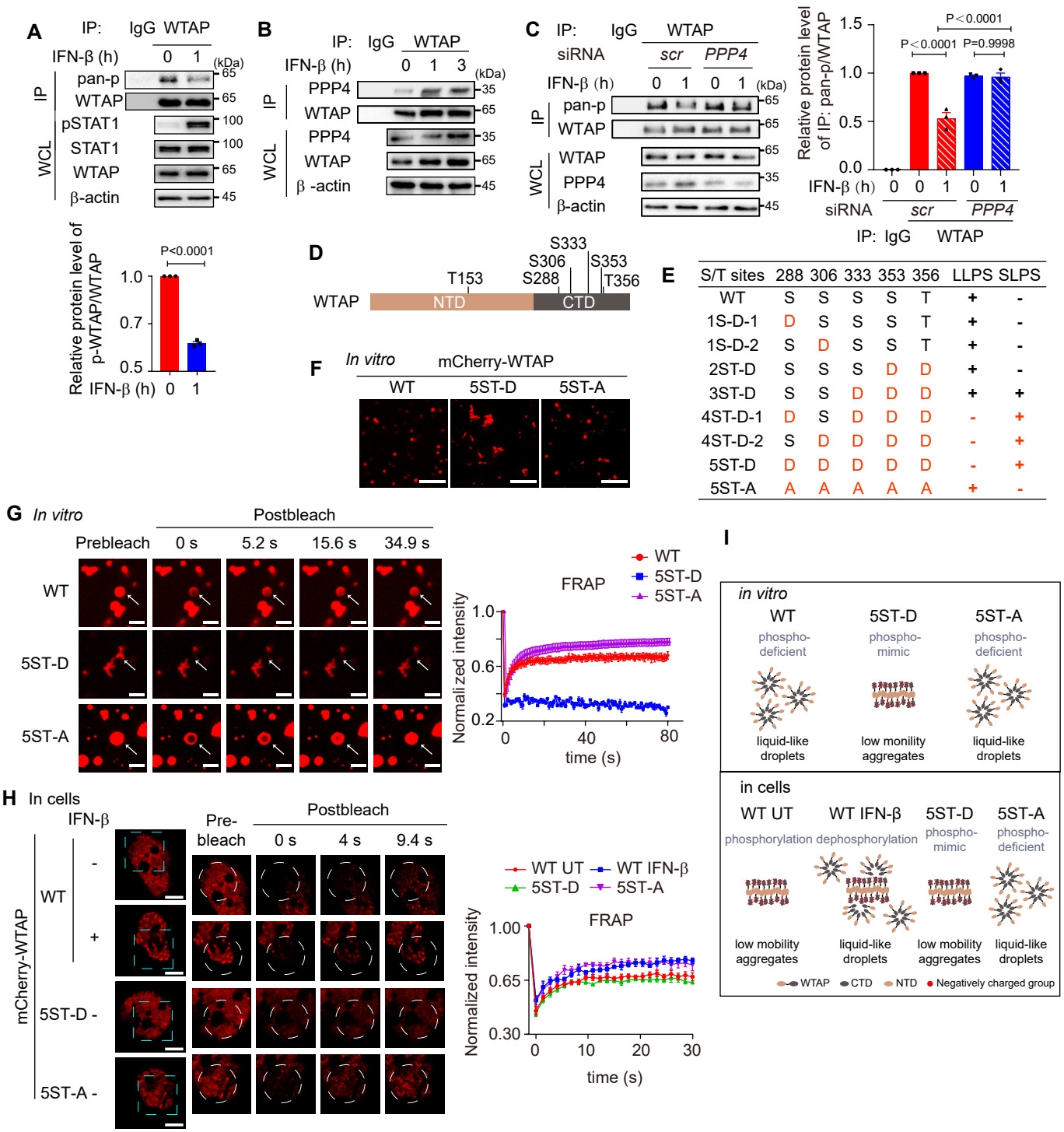

S/T sites	288	306	333	353	356	LLPS	SLPS
WT	S	S	S	S	T	+	-
1S-D-1	D	S	S	S	T	+	-
1S-D-2	S	D	S	S	T	+	-
2ST-D	S	S	S	D	D	+	-
3ST-D	S	S	D	D	D	+	+
4ST-D-1	D	S	D	D	D	-	+
4ST-D-2	S	D	D	D	D	-	+
5ST-D	D	D	D	D	D	-	+
5ST-A	A	A	A	A	A	+	-

Figure 3

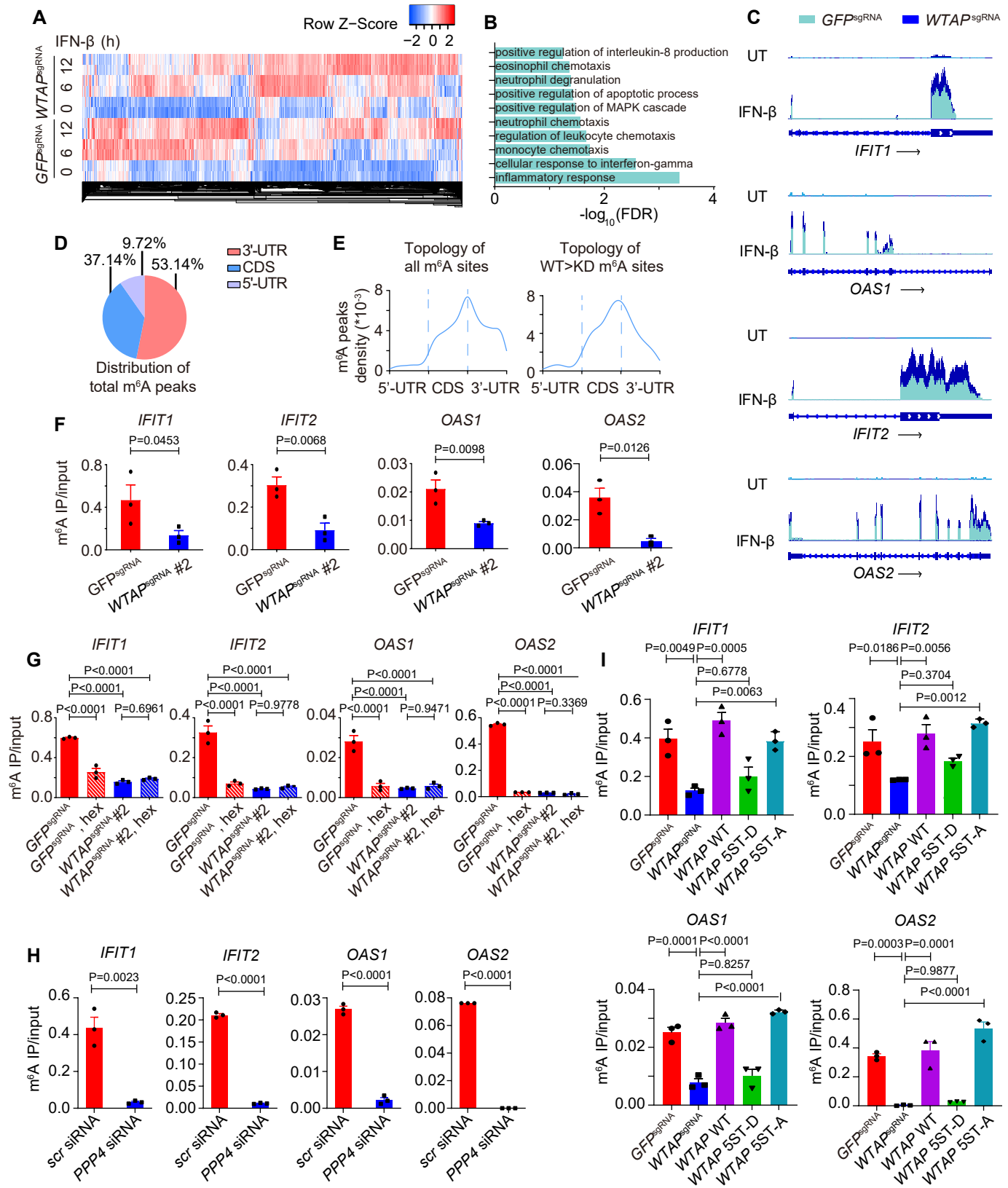
A
Row Z-Score
−2 0 2
IFN-β (h)
WTAP sgRNA
GFP sgRNA
0 6 12 0 6 12
B
positive regulation of interleukin-8 production
eosinophil chemotaxis
neutrophil degranulation
positive regulation of apoptotic process
positive regulation of MAPK cascade
neutrophil chemotaxis
regulation of leukocyte chemotaxis
monocyte chemotaxis
cellular response to interferon-gamma
inflammatory response
0 2 4
-log10(FDR)
C
GFP sgRNA
WTAP sgRNA
UT
IFN-β
IFIT1
OAS1
IFIT2
OAS2
D
9.72%
37.14%
53.14%
3'-UTR
CDS
5'-UTR
Distribution of total m6A peaks
E
Topology of all m6A sites
Topology of WT>KD m6A sites
m6A peaks density (*10-3)
5'-UTR CDS 3'-UTR
F
IFIT1 P=0.0453
IFIT2 P=0.0068
OAS1 P=0.0098
OAS2 P=0.0126
m6A IP/input
GFP sgRNA
WTAP sgRNA #2
G
IFIT1 P<0.0001 P<0.0001 P<0.0001 P=0.6961
IFIT2 P<0.0001 P<0.0001 P<0.0001 P=0.9778
OAS1 P<0.0001 P<0.0001 P<0.0001 P=0.9471
OAS2 P<0.0001 P<0.0001 P<0.0001 P=0.3369
m6A IP/input
GFP sgRNA
GFP sgRNA, hex
WTAP sgRNA #2
WTAP sgRNA #2, hex
I
IFIT1 P=0.0049 P=0.0005 P=0.6778 P=0.0063
IFIT2 P=0.0186 P=0.0056 P=0.3704 P=0.0012
OAS1 P=0.0001 P<0.0001 P=0.8257 P<0.0001
OAS2 P=0.0003 P=0.0001 P=0.9877 P<0.0001
m6A IP/input
GFP sgRNA
WTAP sgRNA
WTAP WT
WTAP 5ST-D
WTAP 5ST-A
H
IFIT1 P=0.0023
IFIT2 P<0.0001
OAS1 P<0.0001
OAS2 P<0.0001
m6A IP/input
scr siRNA
PPP4 siRNA

Figure 4

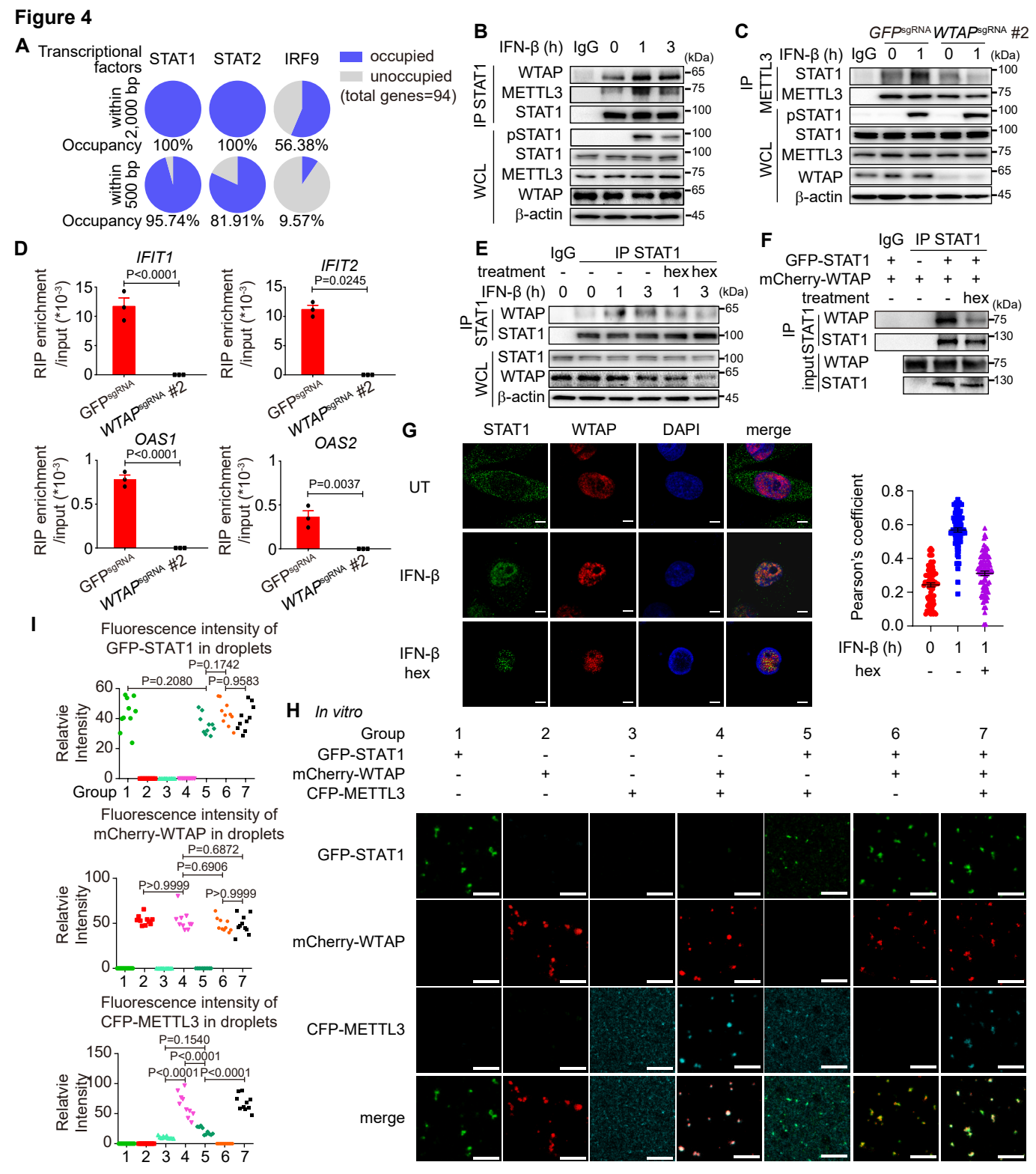
A
Transcriptional factors
STAT1
STAT2
IRF9
occupied
unoccupied
(total genes=94)
within 2,000 bp
Occupancy 100% 100% 56.38%
within 500 bp
Occupancy 95.74% 81.91% 9.57%
B
IFN-β (h) IgG 0 1 3
(kDa)
IP STAT1
WTAP
METTL3
STAT1
WCL
pSTAT1
STAT1
METTL3
WTAP
β-actin
C
GFP sgRNA WTAP sgRNA #2
IFN-β (h) IgG 0 1 0 1
IP
METTL3
STAT1
METTL3
WCL
pSTAT1
STAT1
METTL3
WTAP
β-actin
D
IFIT1
IFIT2
OAS1
OAS2
RIP enrichment /input (*10-3)
P<0.0001
P=0.0245
P<0.0001
P=0.0037
GFP sgRNA
WTAP sgRNA #2
E
IgG IP STAT1
treatment - - - - hex hex
IFN-β (h) 0 0 1 3 1 3
IP STAT1
WTAP
STAT1
WCL
STAT1
WTAP
β-actin
F
IgG IP STAT1
GFP-STAT1 + - + +
mCherry-WTAP + + + +
treatment - - - hex
IP STAT1
input
WTAP
STAT1
G
STAT1 WTAP DAPI merge
UT
IFN-β
IFN-β hex
Pearson's coefficient
IFN-β (h) 0 1 1
hex - - +
H
In vitro
Group 1 2 3 4 5 6 7
GFP-STAT1 + - - - + + +
mCherry-WTAP - + - + - + +
CFP-METTL3 - - + + + - +
GFP-STAT1
mCherry-WTAP
CFP-METTL3
merge
I
Fluorescence intensity of GFP-STAT1 in droplets
P=0.1742
P=0.2080
P=0.9583
Relatvie Intensity
Group 1 2 3 4 5 6 7
Fluorescence intensity of mCherry-WTAP in droplets
P=0.6872
P=0.6906
P>0.9999
P>0.9999
Fluorescence intensity of CFP-METTL3 in droplets
P=0.1540
P<0.0001
P<0.0001
P<0.0001

Figure 5

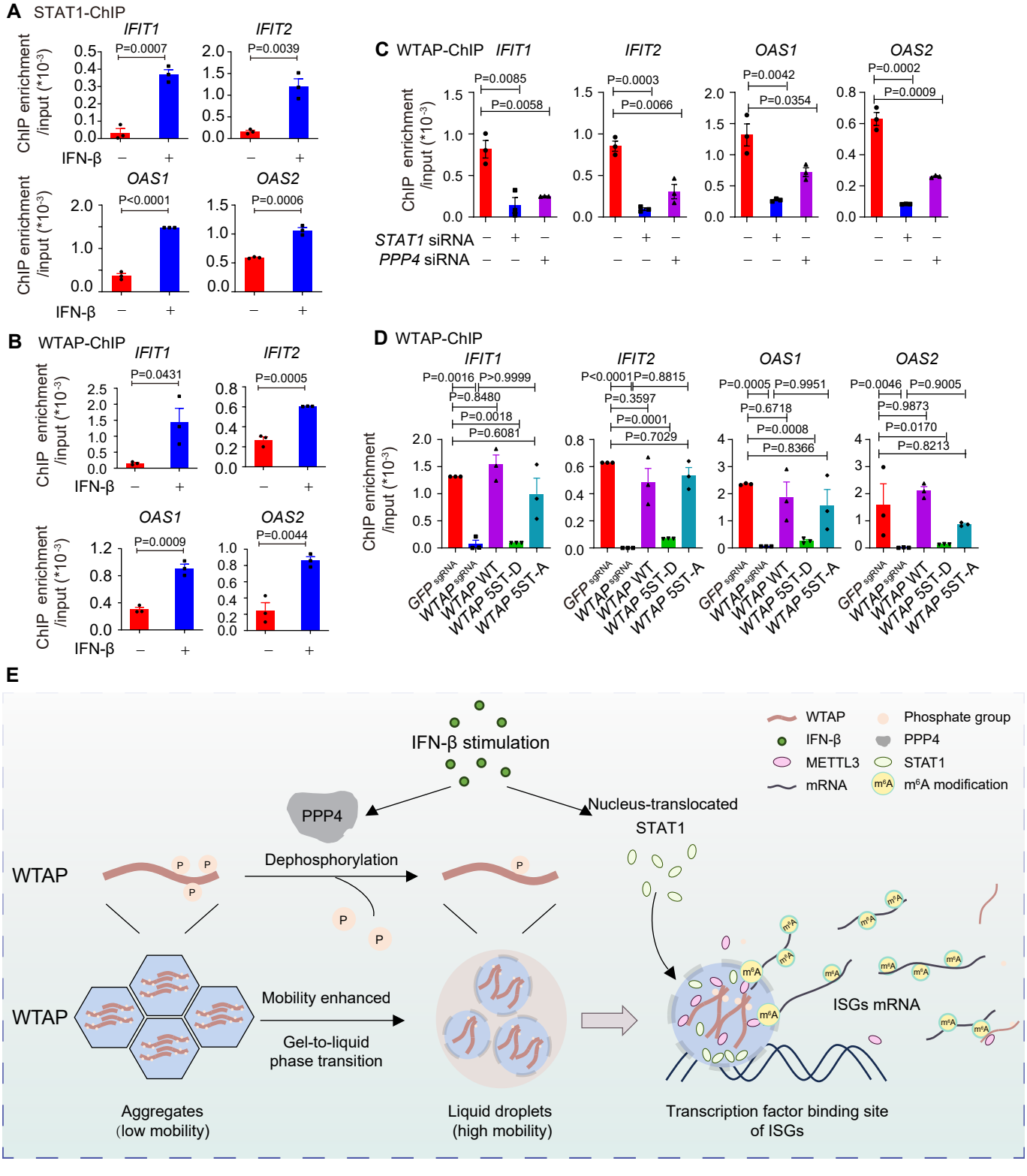
A STAT1-ChIP
IFIT1
IFIT2
OAS1
OAS2
ChIP enrichment /input (*10-3)
P=0.0007
P=0.0039
P<0.0001
P=0.0006
IFN-β
B WTAP-ChIP
P=0.0431
P=0.0005
P=0.0009
P=0.0044
C WTAP-ChIP
P=0.0085
P=0.0058
P=0.0003
P=0.0066
P=0.0042
P=0.0354
P=0.0002
P=0.0009
STAT1 siRNA
PPP4 siRNA
D WTAP-ChIP
P=0.0016
P>0.9999
P=0.8480
P=0.0018
P=0.6081
P<0.0001
P=0.8815
P=0.3597
P=0.0001
P=0.7029
P=0.0005
P=0.9951
P=0.6718
P=0.0008
P=0.8366
P=0.0046
P=0.9005
P=0.9873
P=0.0170
P=0.8213
GFP sgRNA
WTAP sgRNA
WTAP WT
WTAP 5ST-D
WTAP 5ST-A
E
IFN-β stimulation
PPP4
Nucleus-translocated STAT1
WTAP
Phosphate group
IFN-β
PPP4
METTL3
STAT1
mRNA
m6A modification
Dephosphorylation
Mobility enhanced
Gel-to-liquid phase transition
ISGs mRNA
Aggregates (low mobility)
Liquid droplets (high mobility)
Transcription factor binding site of ISGs